FAILURE ANALYSIS OF THICKNESS GRADIENT NEGATIVE POISSON'S RATIO CONCAVE HONEYCOMB SANDWICH PANELS UNDER LOCAL IMPACT

J. H. Xiao[1,2]* and Z. X. Guo[1,2]

Based on the proposed multi-arc curved edge concave adjustable Poisson's ratio cell, five kinds of sandwich panels with negative Poisson's ratio (NPR) were constructed by changing the in-plane thickness of cells: homogeneous, positive gradient, negative gradient, symmetrical positive gradient, and symmetrical negative gradient. The failure mechanical properties of the sandwich panels under the action of local impact were numerically studied. The influences of impact speed and gradient arrangement modes on the failure mode of the sandwich panels, the punch contact force (PCF) and the energy absorption effect (EAE) were investigated. It is found that the failure behavior of sandwich panels is different under different impact speeds. At the same impact speed, the thickness distribution pattern of the sandwich panel core layer will significantly affect the shock resistance of the panel. The study shows that the EAE of sandwich panels can be effectively enhanced by introducing gradient design method, and the sandwich panels with negative gradient arrangement show the best energy absorption effect.

1. Introduction

Honeycomb sandwich-panels structure has obvious advantages in light weight, high bending stiffness and sound insulation [1, 2]. In addition, the ductile deformation of the core layer under impact load also ensures an excellent energy absorption capacity of the sandwich panel [3]. As a protective structure, the sandwich panel has a good application prospect

[1]Department of Engineering Mechanics, Yanshan University, Qinhuangdao 066004, China
[2]Hebei Key Laboratory of Mechanical Reliability for Heavy Equipments and Large Structures, Yanshan University, Qinhuangdao 066004, China
*Corresponding author; e-mail: xiaojunhua@ysu.edu.cn

in automobile, shipbuilding, aerospace, and other industrial fields [4-6]. The deformation of the material with NPR is different from that of the traditional material; under the axial compression load, the material will contact transversely [7, 8]. This special mechanical property makes the material aggregate when subjected to impact, thus enhancing the impact resistance of the material.

The material with NPR is used as the core layer to construct the structure of sandwich panels, that was extensively and deeply studied by many scholars. Duc et al. [9] constructed a conical sandwich shell structure with concave honeycomb material as the core, derived the governing equation of the shell, and analyzed the key factors affecting the critical buckling load of the shell. Quyen et al. [10] studied the nonlinear free and forced vibrations of sandwich cylindrical plates with NPR under explosive loading in thermal environment. Peng et al. [11] analyzed the performance of composite sandwich panels with NPR effect by using the variational progressive multi-scale method and deduced the equivalent panel performance formula of sandwich panels. Cong and Duc [12] proposed a hyperbolic shallow sandwich shell model composed of a negative Poisson's ratio honeycomb core and two panels and studied its nonlinear static stability. Dat et al. [13] proposed the combined model of expanded honeycomb laminate and magnetoelastic panel for the first time and derived the governing equation of its nonlinear vibration problem. Luo et al. [14] compared the shock resistance of sandwich panels with different Poisson's ratios under local impact. Qi et al. [15] numerically studied the mechanical properties of sandwich panels with different Poisson's ratios under projectile impact and found that panels with NPR have the better bullet proof performance. Usta et al. [16] compared the low-speed impact behavior of honeycomb core sandwich panels with four structures through experiments and numerical methods, while the study showed the sandwich panel with NPR has the better EAE with the mount of impact energy. Bohara et al. [17] compared the protective performance of the concave honeycomb sandwich panel with that of the traditional honeycomb sandwich panel and proved that the concave honeycomb sandwich panel has a better protective effect. Xiao et al. [18] proposed a concave hexagonal honeycomb beam and studied the local structural impact response of the beam through experimental and numerical simulation methods. Qi et al. [19] studied the antiknock properties of sandwich panels with concave honeycomb core under the impact load of close proximity and contact explosion through experiments and finite element method (FEM). The finite model provided a good fit to experiment data. Madke and Chowdhury [20] studied the mechanical properties of carbon fiber braided composite sandwich panels with NPR effect under high-speed impact. Lv et al. [21] studied the antiknock performance of the sandwich panel with NPR model based on Voronoi subdivision technology by means of FEM. Chen et al. [22] numerically studied the EAE of double arrow honeycomb sandwich panels under the action of air explosion, and the results showed that the geometric parameters of the cell greatly affect the performance of the structure.

Based on the concept of the gradient structure developed by Lim [23], layered gradient micro-structure design method was introduced into sandwich panel structure. Anh et al. [24] proposed a hybrid sandwich shell model composed of functionally graded graphene sheet reinforced composite layer, dilatant core layer, and functionally graded material layer with reinforcement, and theoretically studied the effects of geometric parameters, material parameters, and reinforcement on the vibrations of the model. Li et al. [25] analyzed the propagation law of stress waves in the gradient honeycomb core and found that the gradient honeycomb core can effectively prevent the propagation of stress waves. Xiao and Zhao [26] analyzed the influence of gradient distribution on the natural frequency of sandwich plates. Dong and Zhang [27] derived the differential equation of motion of honeycomb sandwich plates with NPR under quadrilateral simply supported boundary conditions and analyzed the influence of gradient variation on the natural frequency of the system. Huang et al. [28, 29] studied the static mechanical properties of the lattice sandwich panels with NPR, compared the shock resistance of two kinds of sandwich panels by long straight bar impact test, and found that polyurea coating can increase the EAE of sandwich panels. Fang et al. [30] designed a kind of sandwich panel with gradient honeycomb core, and experimentally studied the three-point bending properties of the plate. Chen et al. [31] experimentally studied the dynamic response of double-arrowhead honeycomb sandwich panels with thickness gradient under blasting and found that the introduction of thickness gradient honeycomb core can heighten the explosion resistance of the plate. Su et al. [32] studied the influence of impact energy and core layer arrangement on the mechanical properties of foam aluminum sandwich panel under explosive loading. Li et al. [33] studied the nonlinear low-speed impact response of 3D lattice sandwich panels with NPR and functional gradient by FEM.
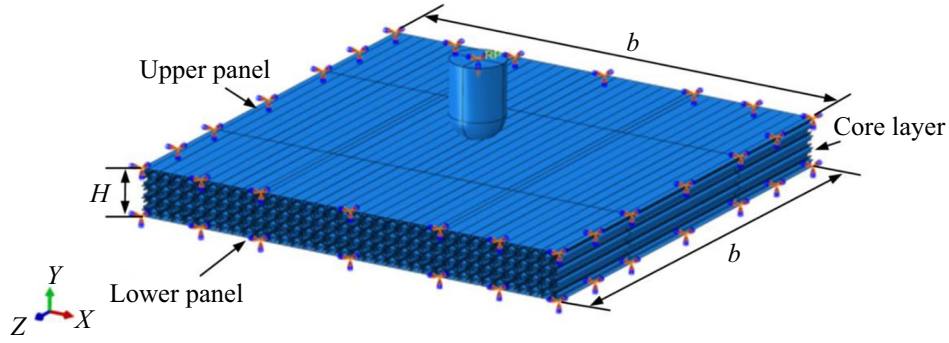
Fig. 1. Schematic diagram of honeycomb sandwich panels with NPR and boundary conditions.
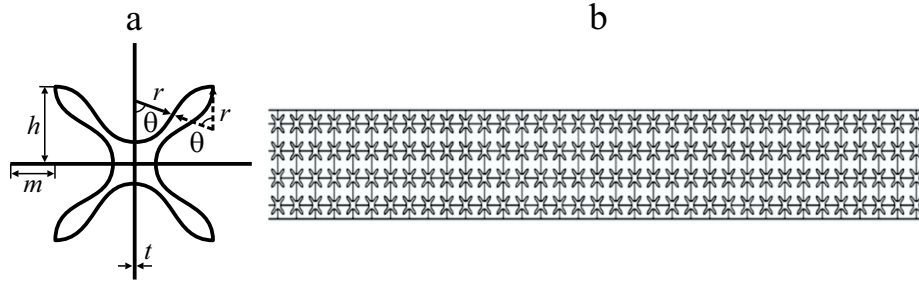

Fig. 2. Concave honeycomb cell with multi-arc curved edge (a) [34] and cross-section of core layer (b).

It can be seen from the existing research that most of current research on the sandwich panels with NPR use concave cells composed of straight rods to construct the core layer of sandwich panels. In this work, based on the proposed multi-curved edge concave adjustable Poisson's ratio cell, the curved concave multicellular structure is constructed as the core layer of sandwich panels. By changing the cell wall thickness of the core layer, five kinds of sandwich panel structures are constructed: homogeneous, positive gradient, negative gradient, symmetric positive gradient, and symmetric negative gradient. The failure behavior of the sandwich panels under local impact was studied, and the impact resistance performance of sandwich panels with different gradients at different impact velocities was analyzed. The research results are a useful supplement to the existing research, and provide a new idea for the subsequent research on NPR sandwich panels.

2. Honeycomb Sandwich Panels with Concave Negative Poisson's Ratio Core

Figure 1 shows the schematic diagram of sandwich panels structure impacted by punch, in which the core layer is constructed based on the concave cell with multi-arc curved edge (Fig. 2a) [34]. The sandwich panels are composed of two panels of the core layer. The core layer is, respectively, provided with "Tie" constraint with the upper and lower panels. The core layer is made up of 4×35 concave cells with multi-arc curved edges (Fig. 2b), and the arc angle is 60°. The remaining structural parameters are taken as follows: h = 1 mm, m = 0.5 mm, H = 12 mm, and b = 105 mm. The punch in Fig. 1 is a hemispherical punch with a diameter of 12.6 mm, length of 20 mm, and mass of 12.25 kg. There is a 1.1-mm gap between the punch and the sandwich panels, which ensures that the punch falls exactly in the center of the sandwich panels. The four sides of the upper and lower panels are fixed, and the punch is allowed to have a displacement in the y-direction. Thus, the punch has a downward directed initial speed. It was used as a universal contact without friction in the tangential direction, and the longitudinal contact is set as rigid contact.

Figure 2a illustrates a multi-arc curved edge concave unit cell with adjustable Poisson's ratio [34], which consists of four curved edges and four extension rods. The cell has five independent parameters: θ, h, m, t, and b, where θ is

TABLE. 1. Core Layer Thickness of Thickness Gradient Sandwich Panels

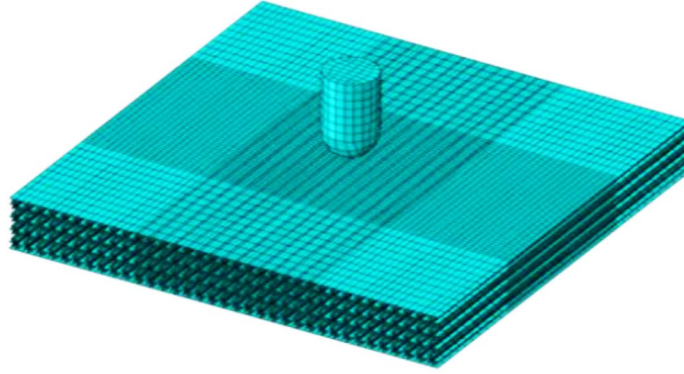| Core layer arrangement mode	T, mm			
	1st layer	2nd layer	3rd layer	4th layer
Homogeneous	0.1	0.1	0.1	0.1
Positive gradient	0.07	0.07	0.13	0.13
Negative gradient	0.13	0.13	0.07	0.07
Symmetric positive gradient	0.13	0.07	0.07	0.13
Symmetrical negative gradient	0.07	0.13	0.13	0.07

Fig. 3. Mesh diagram of sandwich panels and punch.

the arc angle, h is the half-length projected to the coordinate axis by the curved edge of the cell, m is the extension length of the cell connecting rod, t is the in-plane thickness of the rod, b is the out-of-plane thickness of the rod, and radius of the arc edge $r = h/(2\sin\theta)$.

The equivalent Poisson's ratio and the equivalent elastic modulus of the multicellular honeycomb structure are expressed as [34]:

$$v_m = \frac{1 - 4\cos\theta + 3\cos 2\theta - 2\theta\sin\theta - 2\theta\cos\theta + 2\theta + 3\theta\sin 2\theta}{2(3\theta - \theta\sin\theta - \theta\cos\theta + \theta\sin\theta\cos\theta - 2\sin\theta)}, \tag{1}$$

$$E_m = \frac{t^3 E \sin^3\theta}{3h^3 (3\theta - \theta\sin\theta - \theta\cos\theta + \theta\sin\theta\cos\theta - 2\sin\theta)}. \tag{2}$$

Under the condition that the quality of the whole model remains unchanged, the sandwich panels models with five arrangement modes (homogeneous, positive gradient, negative gradient, symmetric positive gradient, and symmetrical negative gradient) are constructed by changing the in-plane thickness t of each layer in the core layer. The thickness of the faceplates is taken as 1 mm. Table 1 shows the wall thickness parameters of five models.

In this work, the low-speed impact simulation of the sandwich panel is carried out by using the explicit dynamics in ABAQUS, and the sandwich panel is analyzed by S4R shell element. The accuracy of simulation is ensured by controlling the "hourglass" phenomenon in finite element analysis, and the artificial strain energy is kept within 5% of the internal energy in this work. The finite element mesh of 45×45 mm in the center of the FEM model is refined (Fig. 3).

In order to verify the correctness of the FEM, the same model as in [35] is constructed in this calculation example. The model parameters and boundary conditions are also consistent with that in [35]. It can be seen from Fig. 4 that the strains of the sandwich panels at different times are consistent with those of existing literature, which confirms the correctness of the FEM model applied in this work.
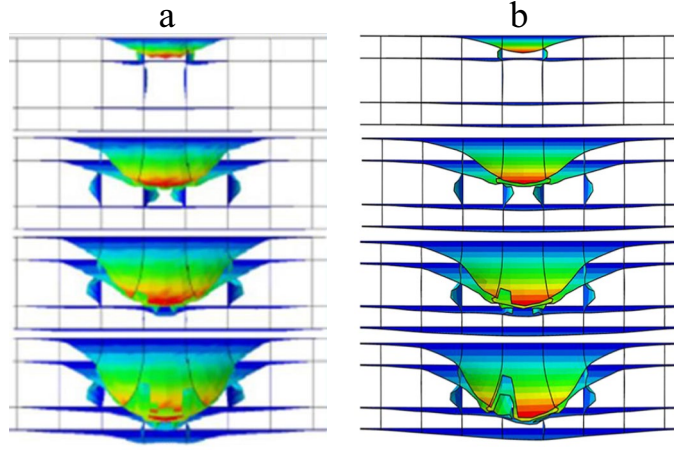
Fig. 4. Comparison of structural deformation calculated in [35] (a) and by present method (b).

3. Material Model of the Constitutive and Failure

The punch is set as a rigid body. The panels and core layer are made of 2024-T3 aluminum alloy [36], with density $\rho = 2700$ kg/m³, elastic modulus $E = 73.1$ GPa, and Poisson's ratio $\mu = 0.33$. In this work, J-C model [37] is adopted, which is often used in impact dynamics simulation.

The expression of yield stress of materials without considering the influence of temperature during the impact is as follows [37]:

$$\sigma_Y = \left(A + B\bar{\varepsilon}_p^n\right)\left(1 + C\ln\dot{\varepsilon}^*\right), \tag{3}$$

where A is the initial yield stress of the material at the reference strain rate $\dot{\varepsilon}_0$, B and n are the hardening modulus and hardening index of the material at the reference strain rate, respectively, C is the material strain rate hardening parameter, $\bar{\varepsilon}_p$ is the effective plastic strain, and $\dot{\varepsilon}^*$ is the strain rate.

The stiffness degradation of the material is simulated by the damage degree D, where $D = 0$ denotes the material is not damaged, and $D = 1$ denotes the material is failed. The degree of damage D can be expressed as [37]:

$$D = \sum \frac{\Delta\varepsilon_p}{\varepsilon^f}, \tag{4}$$

where $\Delta\varepsilon_p$ is the change of equivalent plastic strain within a time step range, ε^f is the failure strain at the current moment [31]:

$$\varepsilon^f = \left[D_1 + D_2\exp\left(D_3\sigma^*\right)\right]\left(1 + D_4\ln\dot{\varepsilon}^*\right), \tag{5}$$

where $D_1, \ldots, D_4$ are the failure parameters of materials, σ^* is the stress triaxiality $\sigma^* = p/\sigma_{\text{eff}}$, where p is the hydrostatic pressure, σ_{eff} is the Von Mises equivalent stress. The material parameters of J-C model of 2024-T3 aluminum alloy are as follows [35]: $A = 369$ MPa, $B = 684$ MPa, $n = 0.73$, $C = 0.0083$, $\dot{\varepsilon}_0/s = 1$, $D_1 = 0.112$, $D_2 = 0.123$, $D_3 = -1.5$, $D_4 = 0.007$.
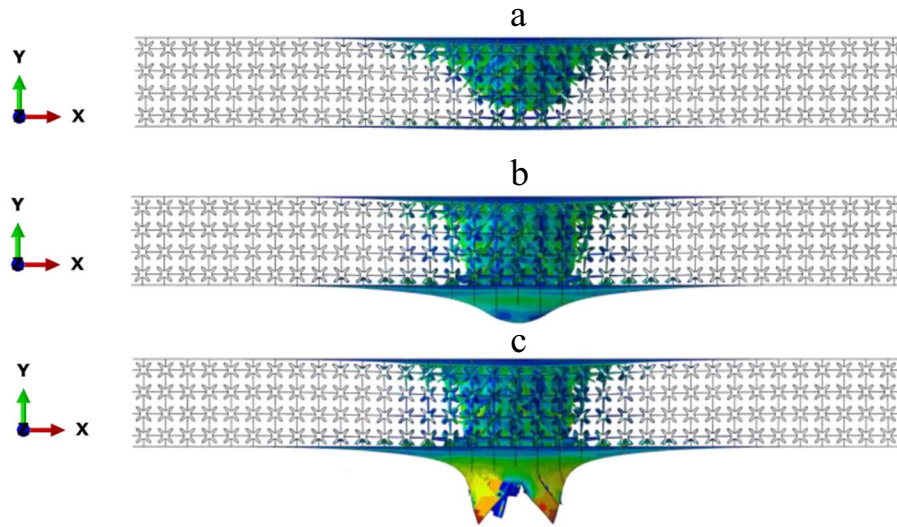
Fig. 5. Failure modes of the homogeneous sandwich panels under different impact speeds: 3 (a), 4 (b), and 5 m/s (c).

4. Effect of Impact Speed on Failure of Sandwich Panels

4.1. Impact failure mode of sandwich panels

Figure 5 shows the failure modes of the homogeneous sandwich panels when the punch contact force is zero under different impact speeds. According to the figure, when the impact speed is 3 m/s, the punch does not contact the lower panel, and the structural deformation mainly occurs in the upper panel and the core. As the impact speed of the punch reaches 4 m/s, the lower panel is extruded by the punch and has serious plastic deformation but is not penetrated. When the impact speed reaches 5 m/s, the lower panel is penetrated.

Figure 6 shows the failure deformation diagrams of homogeneous sandwich panels at different impact times under the impact speed of 5 m/s. It is found that the upper panel cracks when the time reaches 1.8 ms, and the deformation mainly occurs in the upper plate and the core layer. As the impact progresses (3 ms), the upper plate and core begin to lose resistance, while the impact is mainly resisted by the lower panel. Finally, the lower plate reaches the failure limit and is destroyed by impact (at 5 ms).

4.2. Contact force of punch

Figure 7a shows the variation curves of the contact force and displacement of the punch under different impact speeds. It can be seen that the contact force curves of the three impact speeds tend to be consistent when the displacement is small. With the increase of displacement, the contact force rises sharply to a certain peak, and then decreases. Under impact speed of 3 m/s, when the punch displacement reaches 11 mm, the punch contact force (PCF) decreases with the decrease of displacement. The reason is that when the punch reaches this displacement, the speed of the punch decreases to zero and the sandwich panels produces a reaction to the punch, which makes the punch move along the positive direction of the y-axis, and this stage is the rebound stage of the punch. Under the impact velocity of 4 m/s, when the punch displacement reaches 13 mm, the contact force curve decreases to the minimum, and then the PCF starts to increase as the displacement continues to increase. When the punch displacement reaches 19 mm, the PCF reaches another peak, and the punch speed decreases to zero. At this time, under the reaction of the sandwich panels, the punch begins to move in the
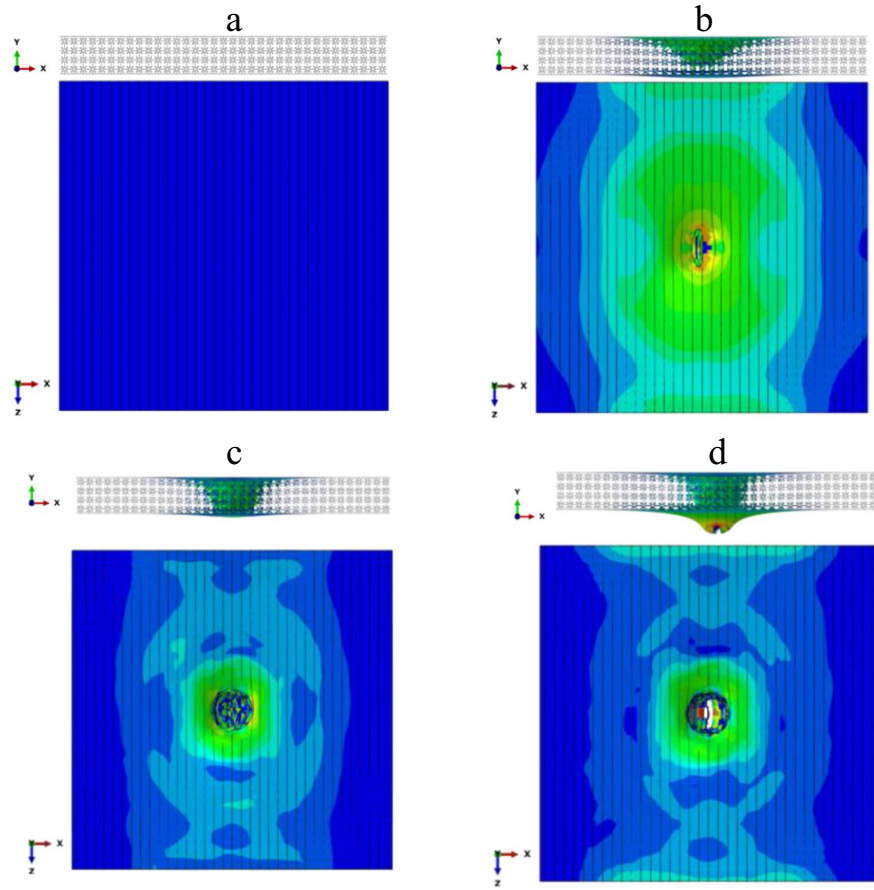
Fig. 6. Failure modes of homogeneous sandwich panels at different impact times: 0 (a), 1.8 (b), 3 (c), and 5.4 ms (d).
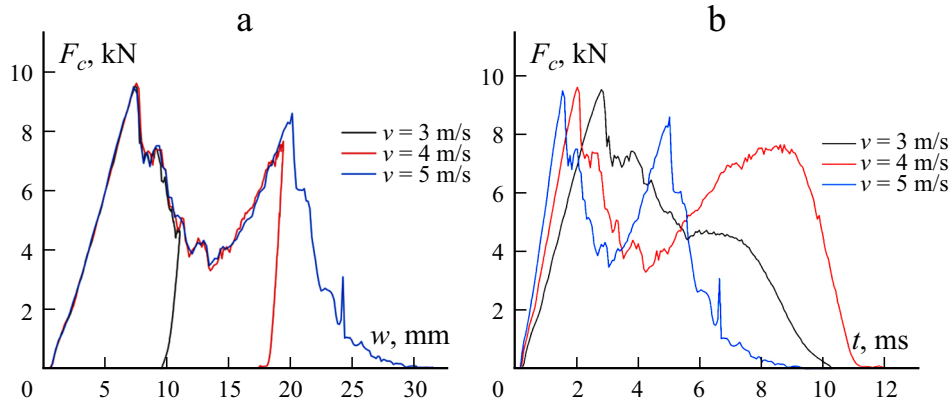

Fig. 7. Changes of punch contact force at different impact speeds: contact force-displacement curve (a) and contact force-time curve (b).

positive direction of y-axis, and the PCF continues to decrease. It can be seen from the diagram that under the impact speeds of 3 and 4 m/s, the contact force displacement curve in the rebound stage of the punch is almost parallel. When the impact speed is 5 m/s, the punch pierces through the sandwich panels, and the second peak of the contact force curve is larger than that of 4-m/s impact. When the curve reaches the second peak, the PCF begins to decrease sharply with the increase of displacement. Figure 7b shows the variation curves of the contact force and time of the punch at different impact
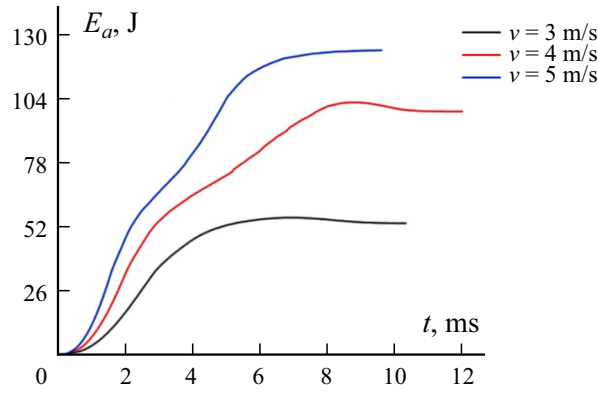
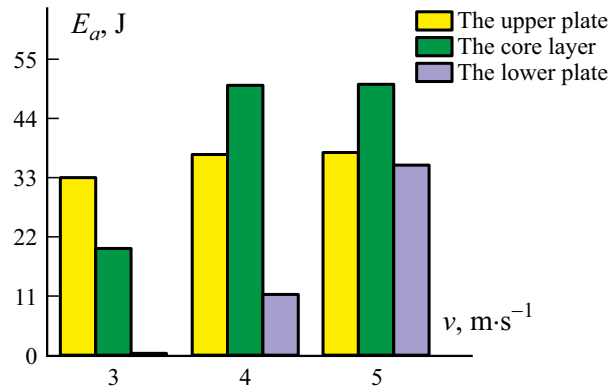Fig. 8. Energy absorption curves at different impact speeds.

Fig. 9. The energy absorption value of each part of sandwich panels at different impact speeds.

speeds. It is shown that the PCF under different impact speeds at the initial stage of impact increases sharply with the increase of time, then starts to decline after rising to a certain value. The slope of the curve increases with the increase of impact speed. When the impact speed is 3 m/s, the slope of the descending section of the curve is smaller than that of the impact speeds of 4 and 5 m/s, and the PCF decreases continuously with the progress of the impact. The curve decreases to a certain value and then begins to rise at the impact speeds of 4 and 5 m/s. When the impact speed is 5 m/s, the slope of the rising section is larger. With further impact, the curve rises to the second peak and then begins to decrease rapidly. The time corresponding to the two peaks of the contact force-time curve under the impact speed of 5 m/s corresponds to the cracking time of the upper panel and the lower panel, respectively. The time, when the PCF begins to rise, twice corresponds to the time of contact between the punch and the upper end panel and the lower end panel, respectively.

4.3. Energy absorption of sandwich panels

Figure 8 shows the time-dependent curves of the energy absorption of the sandwich panels at different impact speeds. It is manifest from the figure that, the energy absorbed by the sandwich plate augments sharply with the progress of the impact, then becomes smooth and tends to be almost constant after reaching a certain time. When the sandwich panel is not punctured (at 3 and 4 m/s), the energy curve decreases slightly in the late impact period. The reason is that the elastic strain energy of the sandwich plate is converted into the kinetic energy of the punch so as to make the punch rebound. The greater the impact speed is, the more energy the sandwich panel absorbs at the same impact time.
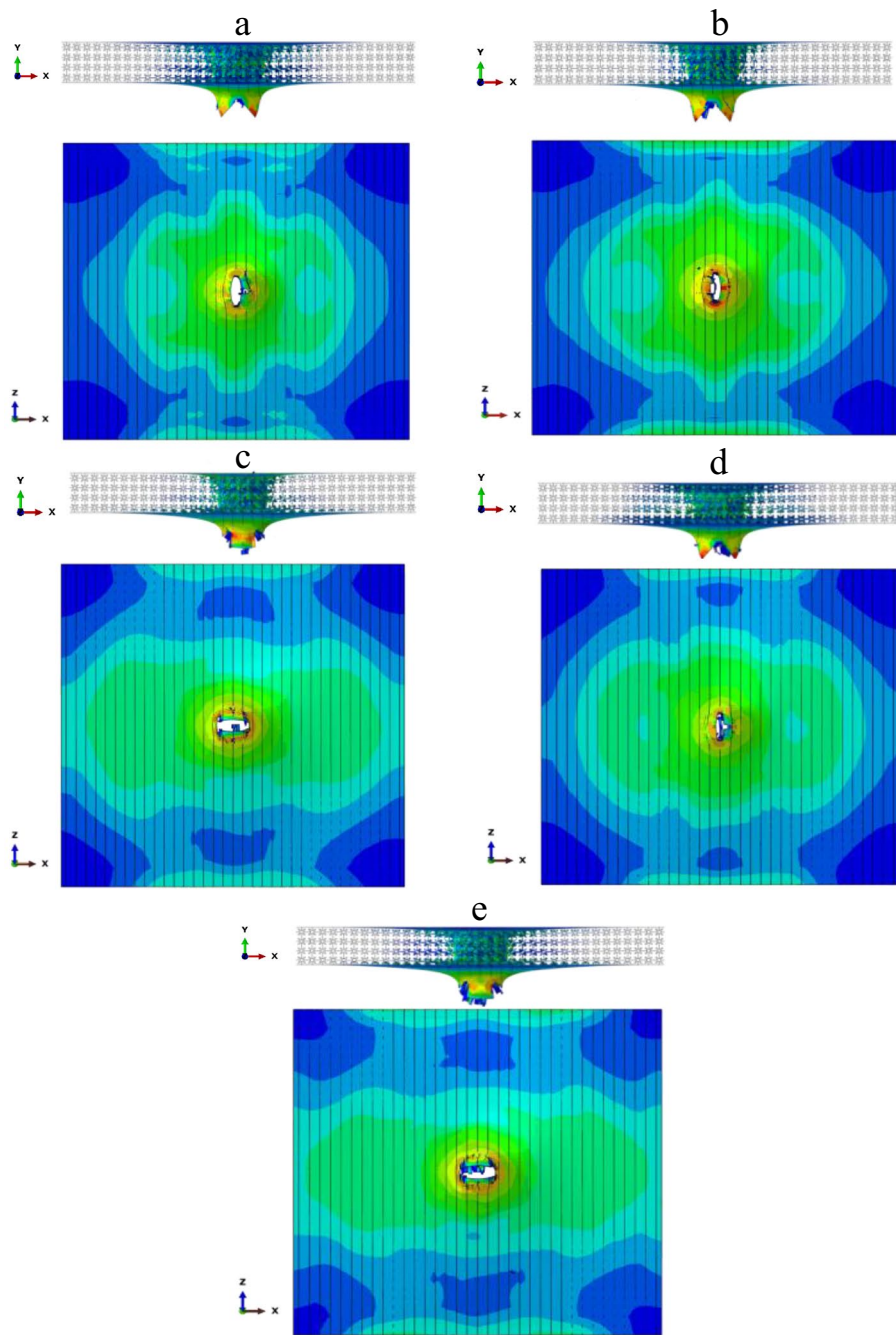
Fig. 10. Failure mode of sandwich panels with different core layer arrangements: homogeneity (a), positive gradient (b), negative gradient (c), symmetric positive gradient (d), and symmetric negative gradient (e).

Figure 9 shows the energy absorption value of each part of the homogeneous sandwich panels when the contact force of the punch is zero at different impact speeds. Under the impact speed of 3 m/s, the impact is mainly resisted by the upper panel, the core layer absorbs a small part of the energy, and the lower panel hardly absorbs energy. As the speed continue to increase (4 m/s), the lower panel deforms significantly, and the core and lower panel absorb a lot of energy, while the upper end plate absorbs energy similar that at the impact of 3 m/s. Under impact speed of 5 m/s, the upper panel and the core layer
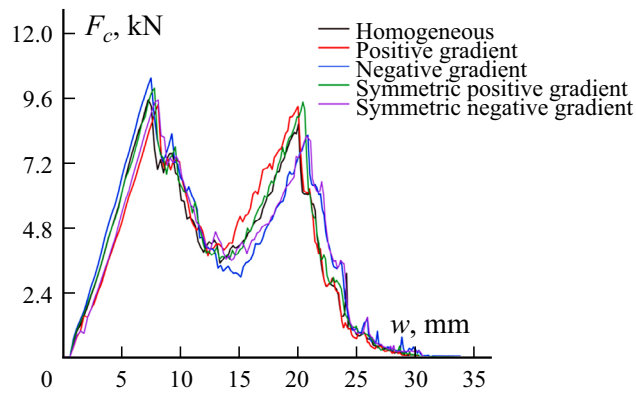
Fig. 11. Contact force-displacement curves for different core layer arrangements.

absorb the same energy as under the impact of 4 m/s since they reach the failure limit, and the energy absorption of the lower panel augments significantly.

5. Effect of Core Layer Arrangement on Failure of Sandwich Panels

5.1. Impact failure mode of the sandwich panels

Figure 10 shows the penetration failure modes of the sandwich panels under impact speed of 5 m/s with different arrangement of the core layer. It is manifest from the figure that, the lower panels of the homogeneous, positive gradient, and symmetrical positive gradient sandwich panels cracked in the z-direction, while the lower panels of the negative gradient and symmetrical negative gradient sandwich panels cracked in the x-direction. The reason is that the cracking mode of the lower panel is related to the wall thickness of the last layer of the core layer: when the bottom wall thickness is small (negative gradient and symmetrical negative gradient), the bottom cell is prone to fracture in the z-direction to form cracks along the x-direction; while the bottom wall thickness is larger (homogeneous, positive gradient and symmetric positive gradient), the outriggers at the lower end of the cell extrude the lower panel to form cracks in the z-direction.

5.2. Contact force of punch

The variation curves of the PCF and displacement of the punch with different arrangement modes of core layer are shown in Fig. 11, where the impact speed is 5 m/s. It is manifest from the figure that, when the sandwich panels with different arrangement are impacted, the PCF changes with displacement are generally consistent. There are two peaks in the contact force-displacement curve, and the first peak is significantly affected by the arrangement mode of core layer. The first peak of the sandwich panel with negative gradient is the largest, while the sandwich panel with positive gradient is the smallest. The second peak is greatly affected by the bottom cell wall thickness of the core layer. The magnitude of the second peak of the positive gradient and the symmetrical positive gradient is almost equal, and they are all larger than those of the homogeneous, negative gradient, and symmetrical negative gradient sandwich panels. The magnitude of the second peak of the negative gradient is almost equal to that of the symmetric negative gradient sandwich panels. It can be found that the second peak of the PCF is mainly affected by the in-plane thickness of the unit cell at the bottom of the core.
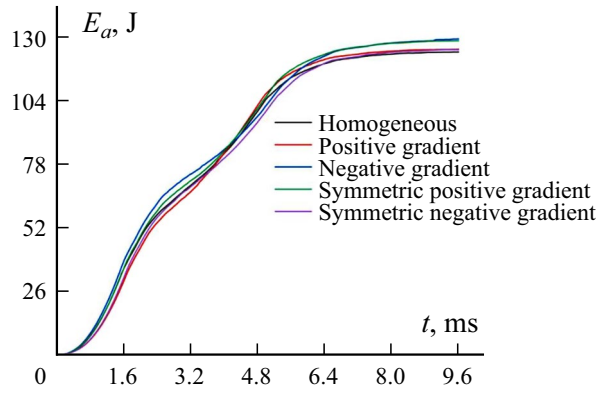
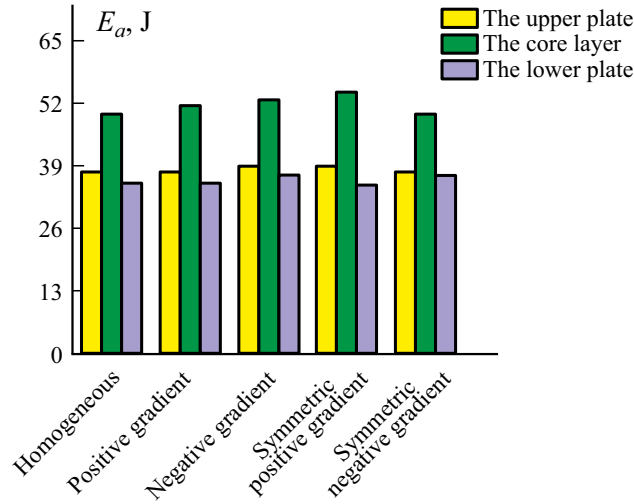Fig. 12. Energy absorption curve of different core layer arrangements.

Fig. 13. Energy absorption of each part of sandwich panels with different core layer arrangements.

5.3. Energy absorption of sandwich panels

Figure 12 shows the time-dependent curves of the energy absorption of the sandwich panels with different core arrangement, where the impact speed is 5 m/s. It is manifest from the figure that; the negative gradient sandwich panels show the better EAE compared with other gradient sandwich panels. When the impact time is less than 4 ms, the EAE of the sandwich panels with negative gradient is the largest. With impact evolution, the sandwich panels is penetrated and the EAE of the sandwich panels with negative gradient is similar to the sandwich panels with symmetrical positive gradient, which is greater than that in other kinds of sandwich panels considered. The EAE of the positive gradient and the symmetric negative gradient sandwich panels are almost identical, and the EAE of the homogeneous sandwich panels is the smallest. It is shown that the EAE of the sandwich panels can be raised by setting the wall thickness arrangement of the core layer.

Figure 13 shows the energy absorption value of each part of the sandwich panels with different core layer arrangement modes when the PCF is zero under the impact speed of 5 m/s. As can be seen from the figure, no matter which kind of the sandwich panels under the impact; the core layer absorbs the most energy, and the energy absorption value by the lower panel is slightly less than that of the upper panel. The research shows that the core with symmetrical positive gradient absorbs the most energy, and the EAE of the upper panel is not significantly affected by the arrangement of the core layer. The EAE of the lower panel is affected by the arrangement of the core layer. The EAE of the lower panel of the negative

gradient and the symmetrical negative gradient sandwich panels are the best. The difference between the energy absorption values of the lower panel of the other three models is small. It can be found comparing the results presented in Fig. 10 that the cracking mode of the lower panel will affect the EAE of the panels.

6. Conclusion

Thickness gradient honeycomb sandwich panels with NPR and concave curved edges were constructed. The failure mechanical properties of sandwich panels under local impact were studied. The effects of impact speed and arrangement mode of core layer on the impact failure properties of the sandwich panels were discussed. The main results are as follows:

The impact failure mode of the sandwich panels depends on the impact speed. When the impact speed is low, the PCF will rebound. Before the rebound stage, the PCF at different impact speeds varies almost the same with displacement. When the punch penetrates the sandwich plate, there are two peaks of the contact force corresponding to the cracking of upper and lower panels, respectively.

With the progress of the impact, the energy absorption value of the sandwich panel augments gradually and tends to be constant slowly after reaching a certain time. At the same time, the energy absorption value augments with the increase of the impact speed.

When the sandwich panels with different arrangement of the core layer are penetrated by impact, the cracking mode of the lower panel is related to the in-plane thickness of the bottom cell wall of the core layer. The contact force curve tends to be consistent, with two peaks. The first peak value is significantly affected by the arrangement of the core layer, while the second peak value is related to the in-plane thickness of the bottom layer of the core layer, which augments with the increase of the in-plane thickness.

The EAE of sandwich panels can be significantly enhanced by setting different in-plane thickness gradient arrangement of the core layer. The negative gradient sandwich panels have the best EAE under impact. The symmetrical positive gradient core layer absorbs the most energy. The energy absorption value of the upper panel is not significantly affected by the arrangement mode of core layer, while the energy absorption value of the lower panel is affected by the arrangement mode of core layer.

REFERENCES

1. Z. Y. Xue and J. W. Hutchinson, "A comparative study of impulse-resistant metal sandwich plates," Int. J. Impact Eng., **30**, No. 10, 1283-1305 (2004).
2. T. Y. Wu and J. W. Wu, "Sound insulation property of honeycomb sandwich panels," Materials Reports, **30**, No. 4, 153-157 (2016) (in Chinese).
3. M. Meo, R. Vignjevic, and G. Marengo, "The response of honeycomb sandwich panels under low-velocity impact loading," Int. J. Mech. Sci., **47**, No. 9, 1301-1325 (2005).
4. V. Birman and G. A. Kardomateas, "Review of current trends in research and applications of sandwich structures," Compos., Part B, **142**, 221-240 (2018).
5. G. Imbalzano, S. Linforth, T. D. Ngo, et al, "Blast resistance of auxetic and honeycomb sandwich panels: Comparisons and parametric designs," Compos. Struct., **183**, 242-261 (2018).
6. G. Imbalzano, P. Tran P, T. D. Ngo, et al, "Three-dimensional modelling of auxetic sandwich panels for localised impact resistance," J. Sandwich Struct. and Mater., **19**, No. 3, 291-316 (2017).

7. X. Ren, X. Y. Zhang, and Y. M. Xie, "Research progress in auxetic materials and structures," Chinese J. Theor. and Appl. Mech., **3**, 656-687 (2019). (in Chinese)

8. L. J. Gibson and M. F. Ashby, "The mechanics of two-dimensional cellular materials," Proc. the Royal Society of London, **382**, No. 1782, 43-59 (1982).

9. N. D. Duc, D. T. Manh, N. D. Khoa, et al, "Mechanical stability of eccentrically stiffened auxetic truncated conical sandwich shells surrounded by elastic foundations," Mech. Compos. Mater., **58**, No. 3, 365-382 (2022).

10. N. V. Quyen, N. V. Thanh, T. Q. Quan, et al, "Nonlinear forced vibration of sandwich cylindrical panel with negative Poisson's ratio auxetic honeycombs core and CNTRC face sheets," Thin Walled Struct., **162**, 107571 (2021).

11. X. Peng, Y. F. Zhou, Z. Shi, et al, "Estimation of effective properties of composite sandwich panels with negative Poisson's ratio by using variational asymptotic multiscale method," Mater. Today Communications, **23**, 101072 (2020).

12. P. H. Cong and N. D. Duc, "Nonlinear thermo-mechanical analysis of ES double curved shallow auxetic honeycomb sandwich shells with temperature-dependent properties," Compos. Struct., **279**, 114739 (2022).

13. N. D. Dat, T. Q. Quan, and N. D. Duc, "Vibration analysis of auxetic laminated plate with magneto-electro-elastic face sheets subjected to blast loading," Compos. Struct., **280**, 114925 (2022).

14. Y. Luo, K. Yuan, L. Shen, et al, "Sandwich panel with in-plane honeycombs in different Poisson's ratio under low to medium impact loads," Reviews on Adv. Mater. Sci., **60**, No. 1, 145-157 (2021).

15. C. Qi, S. Yang, D. Wang, et al, "Ballistic resistance of honeycomb sandwich panels under in-plane high-velocity impact," Scientific World J., **2013**, 892781 (2013).

16. F. Usta, H. S. Turkmen, and F. Scarpa, "Low-velocity impact resistance of composite sandwich panels with various types of auxetic and non-auxetic core structures," Thin-Walled Struct., 163, 107738 (2021).

17. R. P. Bohara, S. Linforth, A. Ghazlan, et al, "Performance of an auxetic honeycomb-core sandwich panel under close-in and far-field detonations of high explosive," Compos. Struct., **280**, 114907 (2022).

18. D. B. Xiao, X. Q. Chen, Y. Li, et al, "The structure response of sandwich beams with metallic auxetic honeycomb cores under localized impulsive loading-experiments and finite element analysis," Materials & Design, **176**, 107840 (2019).

19. C. Qi, A. Remennikov, L. Z. Pei, et al, "Impact and close-in blast response of auxetic honeycomb-cored sandwich panels: experimental tests and numerical simulations," Compos. Struct., **180**, 161-178 (2017).

20. R. R. Madke and R. Chowdhury, "Anti-impact behavior of auxetic sandwich structure with braided face sheets and 3D re-entrant cores," Compos. Struct., **236**, 111838 (2020).

21. W. T. Lv, D. Li, and L. Dong, "Study on blast resistance of a composite sandwich panel with isotropic foam core with negative Poisson's ratio," Int. J. Mech. Sci., **191**, 106105 (2021).

22. G. C. Chen, Y. S. Cheng, P. Zhang, et al, "Design and modelling of auxetic double arrowhead honeycomb core sandwich panels for performance improvement under air blast loading," J. Sandwich Struct. and Mater., **23**, No. 8, 3574-3605 (2021).

23. T. C. Lim, "Functionally graded beam for attaining Poisson-curving," J. Mater. Sci. Letters, 21, 1899-1901 (2002).

24. V. T. T. Anh, N. D. Khoa, T. Ngo, et al, "Vibration of hybrid eccentrically stiffened sandwich auxetic double curved shallow shells in thermal environment," Aerospace Sci. and Technol. 137, 108277 (2023).

25. S. Q. Li, X. Li, G. Y. Wu, et al, "Dynamic response of functionally graded honeycomb sandwich plates under blast loading," Explosion and Shock Waves, **36**, No. 3, 333-339 (2016) (in Chinese).

26. D. B. Xiao and G. P. Zhao, "Vibration response of sandwich panels with gradient metallic cellular core," Acta Aeronautica et Astronautica Sinica, **38**, No. 6, 220576 (2017) (in Chinese).

27. B. J. Dong and J. H. Zhang, "Vibrations of functional graded honeycomb sandwich plate with negative Poisson's ratio," Sci. Technol. and Eng., **19**, No. 21, 110-116 (2019) (in Chinese).

28. X. F. Huang and Z. H. Zhang, "Static mechanical properties of three-dimensional polyurea-coated lattice structures with negative Poisson's ratio," Scientia Sinica: Physica, Mechanica & Astronomica, **51**, 054601 (2021) (in Chinese).

29. X. F. Huang, Z. H. Zhang, and J. H. Wu, "Dynamic response tests of polyurea-coated 3-D lattice sandwich structure with negative Poisson's ratio under impact load," J. Vibration and Shock, **40**, No. 17, 259-270 (2021) (in Chinese).

30. G. Fang, S. Yuan, S. Meng, et al, "Graded negative Poisson's ratio honeycomb structure design and application," J. Sandwich Struct. and Mater., **21**, No. 7, 2527-2547 (2019).

31. G. C. Chen, Y. S. Cheng, P. Zhang, et al, "Blast resistance of metallic double arrowhead honeycomb sandwich panels with different core configurations under the paper tube-guided air blast loading," Int. J.. Mech. Sci., **201**, 106457 (2021).

32. X. Y. Su, L. Jing, and L. M. Zhao, "Failure modes and shock resistance of sandwich panels with layered-gradient aluminum foam cores under air-blast loading," Explosion and Shock Waves, **39**, No. 6, 063103-1-063103-8 (2019).

33. C. Li, H. S. Shen, J. Yang, et al, "Low-velocity impact response of sandwich plates with GRC face sheets and FG auxetic 3D lattice cores," Eng. Analysis with Boundary Elements, **132**, 335-344 (2021).

34. Z. X. Guo and J. H. Xiao, "Mechanical properties of multi-arc concave honeycomb structure with adjustable Poisson's ratio," Eng. Mech., doi: 10.6052/j.issn.1000-4750.2022.01.0093 (2022) (in Chinese).

35. S. L. Cheng, H. Y. Yang, C. Geng, et al, "Study on the sinusoidal honeycomb core metamaterial sandwich panel with high-performance and low-velocity impact resistance," Appl. Physics A-Mater. Sci. and Processing, **128**, No. 12, 1092 (2022).

36. D. Lesuer, "Experimental investigations of material models for Ti-6A1-4V and 2024-T3," San Francisco: Lawrence Livermore National Laboratory, (1999).

37. G. R. Johnson and W. H. Cook, "Fracture characteristics of three metals subjected to various strains, strain rates, temperatures and pressures," Eng. Fracture Mech., **21**, No. 1, 31-48 (1985).